Vortex dynamics in two-dimensional systems at high driving forces

Hans Fangohr,[1,2] Simon J. Cox,[1] and Peter A. J. de Groot[2]
[1]*Department of Electronics and Computer Science, University of Southampton, Southampton SO17 1BJ, United Kingdom*
[2]*Department of Physics and Astronomy, University of Southampton, Southampton SO17 1BJ, United Kingdom*
(Received 17 October 2000; published 18 July 2001)

We study numerically the dynamics of two-dimensional vortex systems at zero temperature. In addition to pinned states and turbulent plastic flow, we find motion of vortices in rough channels along the direction of the driving force. In this decoupled channel regime we demonstrate how topological defects mediate the phase slip of different channels moving with different velocities. We thus provide important confirmation of recent analytical work describing vortex dynamics at high driving forces such as the moving glass theory of Giamarchi and Le Doussal. For the largest driving forces we find that the channels couple and observe elastic motion.

DOI: 10.1103/PhysRevB.64.064505 PACS number(s): 74.60.Ge, 64.60.Cn, 05.70.Ln

I. INTRODUCTION

Vortex dynamics in the presence of disordering pinning show a variety of nonequilibrium physics and dynamic phase transitions. Experiments,[1–7] numerical,[8–12] and analytical[13–18] work suggest that a disordered static system of vortices shows ordering at higher driving forces. Koshelev and Vinokur[13] predicted a dynamic phase transition between plastic sliding for driving forces just above depinning and coherent motion of crystalline structures at high driving forces. Subsequently, Giamarchi and Le Doussal[14] predicted that the strongly driven and reordered system would be a moving glass, where vortices move elastically-coupled along static channels, such that they flow in the direction of the driving force along well-defined, nearly parallel paths in the pinning potential. These optimal channels (in two dimensions) or sheets (in three dimensions) show a roughness and are predicted to be a static and reproducible feature of the disorder configuration.

Balents, Marchetti, and Radzihovsky argued[15] that in addition to elastically-coupled channels (no topological defects in the system) at intermediate velocities a transverse-moving smectic[15,16] would exist in which motion of vortices in different channels is decoupled (topological defects between the channels). Later work[16–18] mainly supported the initial findings of Giamarchi and Le Doussal with the addition of the moving smectic as predicted by Balents, Marchetti and Radzihovsky.[15] Different names are in common use: the moving transverse glass[18] (MTG), moving smectic[16] and decoupled channels[17] refer to the decoupled channel motion, and the moving Bragg glass[18] (MBG), moving lattice[16] and coherent phase[17] refer to the regime of elastically coupled channels.

The theoretical descriptions[14–18] of these dynamic phases are based on elastic theory and assume either the absence (for the MBG) or the irrelevance (for the MTG) of topological defects. In fact, the theory of Giamarchi and Le Doussal[14,18] describes both regimes with the same equation, which is (nearly) exact for the MBG and remains an effective description for the MTG. In this work we investigate the role of topological defects in the MTG to check the validity of assumptions entering the theory of Giamarchi and Le Doussal, and find them to be justified.

We review the dynamic phase diagram for a two-dimensional 2D vortex system in the presence of random disorder varying on a length scale much smaller than the vortex-vortex spacing. Our model describes rigid vortices in thin films or decoupled pancake vortices in layered materials. We employ a modified cutoff[19] to the appropriate interaction force that corresponds to a logarithmic vortex-vortex interaction potential.[20] After annealing a vortex system to zero temperature, we apply an increasing driving force and study the dynamics of the system systematically for different pinning strengths.

Section II describes the simulation and the computational details. In Sec. III we present a dynamic phase diagram and give an overview of the observed dynamic phases (III A). These phases are a pinned vortex glass (III B), different kinds of turbulent plastic flow (III C), a decoupled channel regime (III D), and coherently moving structures (III E). In Sec. IV we consider the decoupled channel regime in detail: we report on the dependence of the spatial distribution of velocities in the different channels on the pinning landscape (IV A), we show how topological defects between the channels mediate the phase slip between channels while preserving the transverse periodicity of the system (IV B), and we give information on the transverse depinning in the decoupled channel regime (IV C). Finally, we draw our conclusions in Sec. V. The Appendix contains technical information on the smooth cutoff used.

II. THE SIMULATION

A. Equation of motion

We consider a two-dimensional vortex system and model the vortex motion with overdamped Langevin dynamics. The total force $\mathbf{F}_i$ acting on vortex i is given by

$$\mathbf{F}_i = -\eta \mathbf{v}_i + \mathbf{F}^{\mathrm{L}} + \mathbf{F}_i^{\mathrm{vv}} + \mathbf{F}_i^{\mathrm{vp}} + \mathbf{F}_i^{\mathrm{therm}} = \mathbf{0}, \tag{1}$$

where η is the Bardeen-Stephen[21] viscosity coefficient, $\mathbf{v}_i$ the velocity, $\mathbf{F}^{\mathrm{L}}$ the Lorentz force acting equally on all vortices, $\mathbf{F}_i^{\mathrm{vv}}$ the vortex-vortex interaction, $\mathbf{F}_i^{\mathrm{vp}}$ the vortex-pinning interaction, and $\mathbf{F}_i^{\mathrm{therm}}$ a stochastic noise term to model temperature.[22] The vortex-vortex interaction force for rigid vortices in thin films and pancakes in decoupled layers of multilayer materials experienced by vortex i at position $\mathbf{r}_i$ is[20]

$$\mathbf{F}_i^{vv} = \frac{\Phi_0^2 s}{2\pi\mu_0\lambda^2} \sum_{j\neq i} \frac{\mathbf{r}_i - \mathbf{r}_j}{|\mathbf{r}_i - \mathbf{r}_j|^2}. \quad (2)$$

The constant Φ_0 is the magnetic flux quantum, s the length of the vortex, μ_0 the vacuum permeability, and λ the London penetration depth. We employ periodic boundary conditions and cut off the logarithmic vortex-vortex repulsion potential smoothly.[19] The important feature of this modified interaction potential is that it does not introduce numerical artifacts, such as topological defects that can result from using a naive cutoff potential. Details can be found in the Appendix and Ref. 19. The cutoff distance is $\min(L_x/2, L_y/2)$ where L_x and L_y are the lengths of the sides of the rectangular simulation cell. The lengths L_x and L_y are chosen such that a hexagonal lattice fits perfectly in the simulation cell.

We investigate systems with a magnetic induction of $B = 1$ T and a penetration depth of $\lambda = 1400$ Å that yields a vortex density of $\approx 10/\lambda^2$ representative of typical cuprate superconductors. The random pinning potential we have employed varies smoothly on a length scale of $\lambda/25$, which is of the order of the coherence length ξ. This is a representation of random pinning on the atomic length scale (for example, due to oxygen vacancies or small clusters of oxygen vacancies) since the vortex cores effectively smooth the pinning potential over a length scale of the core diameter 2ξ. Fig. 1(a) demonstrates the construction of the pinning potential in one dimension. Figure 1(b) shows a part of the pinning structure used for the two-dimensional system. System sizes from 100 to 3000 vortices have been investigated. We measure lengths in units of $\lambda = 1400$ Å, and forces in units of the force f_0 that two vortices separated by λ experience. We express time in units of $t_0 = \eta\lambda/f_0 = \eta 2\pi\mu_0\lambda^4/\Phi_0^2 s$ which is in line with other simulations.[10,23]

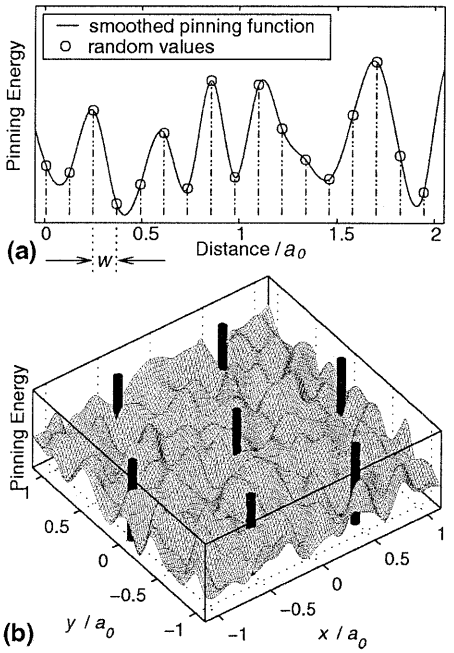

FIG. 1. A sample pinning potential. Distances are given in multiples of the vortex lattice spacing, a_0. (a) Demonstration of construction of the pinning potential in one dimension: First, we assign random pinning energies at discrete sites (shown as open circles) with spacing w. Secondly, we interpolate between those sites using cubic splines to obtain an effectively continous pinning potential. This results in a random pinning potential with a short-range correlator $\overline{V(r)V(r')} = g(r-r')$ of range w. We follow an analogous procedure in two dimensions. (b) A part of a pinning potential as used in the simulations. The seven black cylinders indicate vortex lines separated by a_0 to demonstrate the length scale.

B. Observables

To distinguish different dynamic phases we monitor the topological defect density n_d (defined as the fraction of vortices with less or more than six nearest neighbors in the Delaunay triangulation[24]) and the distribution $\Gamma(\langle v\rangle)$ of time-averaged velocities $\langle v_i\rangle(t) = |[\mathbf{r}_i(t+t_0) - \mathbf{r}_i(t_0)]/t|$ of individual vortices i over time t. We also observe the structure factor of the system (the Fourier transform of the vortex positions), a measure for local hexagonal order (using bond angles θ_k from the Delaunay triangulation we compute $\Psi_6 = (1/n_{\text{bond}})|\Sigma_{k=1}^{n_{\text{bond}}} \exp(i6\theta_k)|$, where n_{bond} is the number of angles in the Delaunay triangulation), the frequency spectrum of the center-of-mass velocity, and the paths of motion of vortices (two-dimensional histogram of vortex positions). We create movies of time snap-shots of vortex positions to visualize the behavior of the system.

III. THE DYNAMIC PHASES

Initially, we anneal the vortex system from a molten state to zero temperature in the presence of the random pinning potential. The pinning forces are obtained by numerically differentiating the potential. The root mean square value of the pinning force field is denoted by $F_{\text{rms}}^{\text{vp}}$. An annealed vortex configuration is shown in Fig. 2. After annealing, a driving force is applied that is subsequently increased every 4×10^4 time steps. This yields force-velocity characteristics that correspond to experimentally obtainable current-voltage characteristics (at zero temperature). The driving force $\mathbf{F}^{\text{L}}$ is related to the current density $\mathbf{j}$ via $\mathbf{F}^{\text{L}} = s\mathbf{j}\times\mathbf{\Phi}_0$, and the vortex velocity to the induced electric field $\mathbf{E}$ via $\mathbf{E} = \mathbf{B}\times\mathbf{v}$, where $\mathbf{B}$ is the magnetic induction and $\mathbf{v}$ the vortex velocity. We investigate the modes of motion at different driving forces and pinning strengths using the observables specified in Sec. II B.

A. The phase diagram

The different observed modes of plastic and elastic motion are summarized in Table I. The second column of the table shows the expressions used for each mode of motion and a reference to the section in which it is described. The third and fourth columns show the criterion used to identify and distinguish the modes, and the fifth column gives further observations.

We describe now briefly the phase diagram shown in Fig. 3. For weak pinning ($F_{\text{rms}}^{\text{vp}} \lesssim 0.8 f_0$) a pinned vortex glass

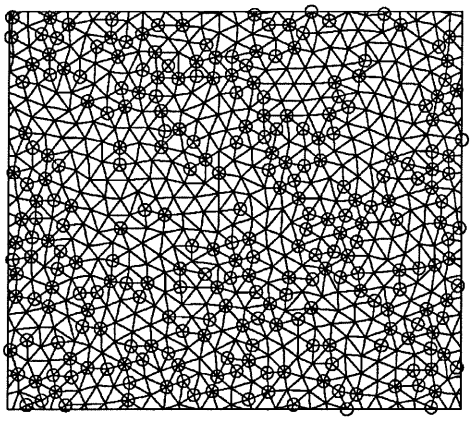

FIG. 2. A pinned vortex glass at pinning strength $F_{\mathrm{rms}}^{\mathrm{vp}}=1.2f_0$. The system has been annealed from molten to zero temperature. The figure shows the Delaunay[24] triangulation of vortex positions. Here, $n_{\mathrm{d}}=0.46$, i.e., 46% of the 576 vortices are topological defects (having more or less than six nearest neighbors) and are highlighted by open circles.

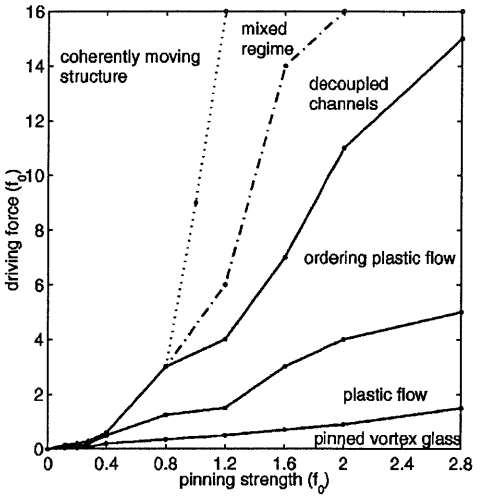

FIG. 3. Dynamic phase diagram of the vortex state as a function of disordering pinning strength $F_{\mathrm{rms}}^{\mathrm{vp}}$ and strength of the driving force (at zero temperature).

(Fig. 2) undergoes plastic flow (PF) and ordering plastic flow (OPF) for an increasing driving force (Sec. III C). In OPF, in contrast to PF, the density of topological defects, n_{d}, is lower than the density of the static system, $n_{\mathrm{d}}^{\mathrm{static}}$. We summarize PF and OPF as turbulent plastic flow because in both modes the motion of vortices is turbulent rather than laminar, i.e., the motion of different vortices is hardly correlated. This helps us to distinguish between the turbulent (chaotic) plastic flow of PF and OPF and the (laminar) plastic motion of vortices in the decoupled channel regime (Sec. III D, Sec. IV). At high driving forces the vortices move elastically as a coherently moving structure, i.e., every vortex keeps its nearest neighbors for all times (Sec. III E).

For the weakest pinning strength of $F_{\mathrm{rms}}^{\mathrm{vp}}\approx 0.04f_0$ the annealed system is a defect-free Bragg glass[25] and changes directly from the pinned Bragg glass to MBG (Ref. 14) without undergoing plastic motion. However, since the initial configuration is annealed from random positions, this MBG is, in general, not aligned with the direction of the driving force, and the pinning is too weak to reorientate it. This very

TABLE I. Overview of observed plastic and elastic modes of motion. $\Gamma(\langle v\rangle)$ is the distribution of time-averaged vortex velocities, and n_{d} is the density of topological defects (Sec. II B). The topological defect density of the annealed system without any applied driving force is $n_{\mathrm{d}}^{\mathrm{static}}$.

	Name	Criterion		Observations
		$\Gamma(\langle v\rangle)$	n_{d}	
Plastic modes	PF and some vortices permanently pinned Sec. III C	Broad, and peak at zero	$n_{\mathrm{d}}\geqslant n_{\mathrm{d}}^{\mathrm{static}}$	Turbulent flow, system partly pinned.
	PF and no vortices permanently pinned Sec. III C	Broad	$n_{\mathrm{d}}\geqslant n_{\mathrm{d}}^{\mathrm{static}}$	Turbulent flow, peak at zero in instantaneous velocity distribution (i.e., some stationary vortices).
	OPF Sec. III C	Broad	$n_{\mathrm{d}}<n_{\mathrm{d}}^{\mathrm{static}}$	Turbulent flow, no vortices have zero velocity in instantaneous velocity distribution $\Leftrightarrow$ "crinkle motion" (i.e., all vortices moving).
	Decoupled channels, MTG Sec. IV	Separated δ peaks	$0<n_{\mathrm{d}}\ll n_{\mathrm{d}}^{\mathrm{static}}$	Motion in uncoupled channels in direction of driving force, topological defects between channels, critical transverse force.
Elastic modes	Coherently moving structure without defects, MBG, Sec. III E	Single δ peak	$n_{\mathrm{d}}=0$	Motion in coupled channels in direction of driving force, washboard frequency in noise spectrum, critical transverse force.
	Coherently moving structure with defects, Sec. III E	Single δ peak	$0<n_{\mathrm{d}}\ll n_{\mathrm{d}}^{\mathrm{static}}$	Vortices generally aligned with the direction of the driving force

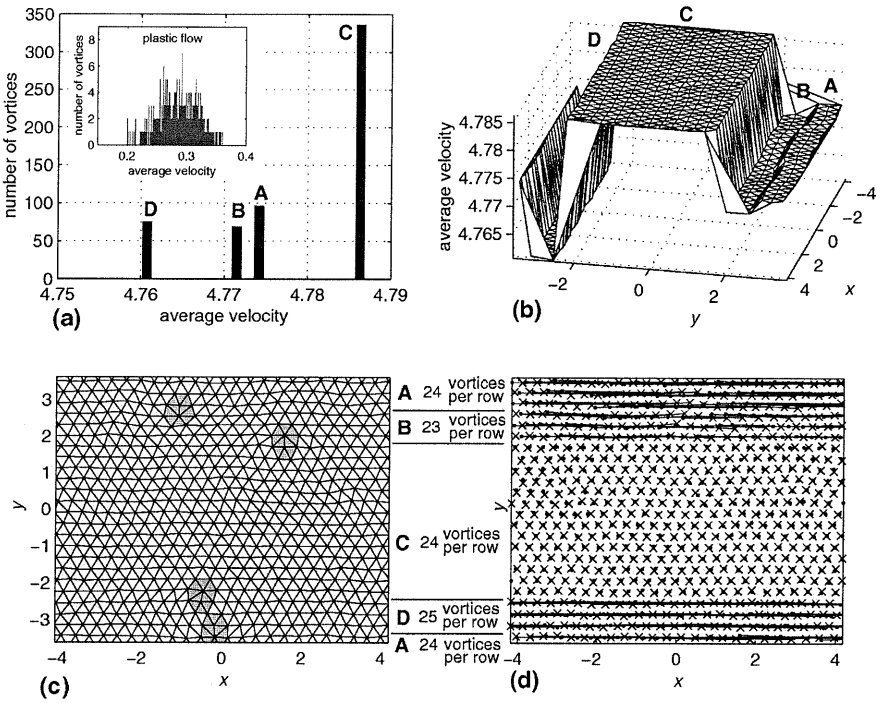

FIG. 4. The decoupled channel regime. Periodic boundary conditions are applied in x and y directions. (a) Velocity histogram of time-averaged individual vortex velocities $\Gamma(\langle v \rangle)$ for a driving force $F_x^{\mathrm{L}} = 5.0 f_0$. Inset: same for turbulent plastic flow with $F_x^{\mathrm{L}} = 0.9 f_0$. (b) Delaunay triangulation of one time step with the time-averaged individual vortex velocity plotted in the third dimension. There are four distinct groups labeled A, B, C and D of vortex-channels traveling along the x direction with different velocities. (c) Two-dimensional view of (b) and topological defects are highlighted. (d) Change between initial (●) and final (×) vortex positions in the frame of reference of one of the vortices in group C.

weak pinning regime has not been studied in detail in the framework of this investigation.

For stronger pinning ($F_{\mathrm{rms}}^{\mathrm{vp}} \gtrsim 0.8 f_0$) there is an intermediate regime between turbulent plastic flow and coherently moving structures in which rows of vortices are aligned with the driving force and vortices move in preferred channels. However, these channels are decoupled: vortices in different channels move with different velocities (Sec. IV). The change from the decoupled channel regime to a coherently moving structure depends on the history of the system: in the mixed regime both modes of motion can be found depending on whether the driving force is increased or decreased.

Related numerical work on dynamic phases has been performed by Moon, Scalettar and Zimányi,[9] Ryu *et al.*[10] and Olson, Reichhardt and Nori.[12] It was found in Ref. 9 that as the driving force is increased, first the pinned vortex glass exhibits plastic flow and finally moves as a "moving glass" that is very likely to be the decoupled channel regime. Ref. 10 found an elastically moving structure with topological defects at high driving forces. In contrast to this work in which we have used logarithmic interactions and have varied the strength of the pinning forces, in Ref. 12 the strength of an exponentially decaying vortex-vortex interaction has been varied in a system with a smaller vortex density. However, the results can be compared qualitatively, and Ref. 12 demonstrates similar findings on plastic flow, decoupled channels and coupled channels.

B. Pinned vortex system

For sufficiently small driving forces the system is pinned and the velocity distribution shows a single peak at zero velocity. For pinning strengths above $\approx 0.04 f_0$ we see the number of topological defects increasing with pinning strength and no long-range order exists. We thus refer to the pinned system as a vortex glass, and such a configuration is shown in Fig. 2.

C. Turbulent plastic flow

Vortices start moving if the driving force exceeds a critical value. We distinguish two different kinds of motion, which we refer to as PF and OPF. Both types of motions show a broad distribution of time-averaged vortex velocities as shown in the inset in Fig. 4(a), which, for very small driving forces, has another peak at zero velocity. We call the motion OPF if the density of topological defects, n_{d}, is below the defect density, $n_{\mathrm{d}}^{\mathrm{static}}$, the system would have if no driving force was applied. Otherwise we call it PF (Table I).

We observe PF for driving forces just above the critical depinning force. The topological defect density is higher than for the static system because some vortices are stationary and others are squeezing past them. Within the PF regime we find two modes of motion: For driving forces just above the depinning current we find a bimodal distribution in the time-averaged vortex velocity showing a peak at zero velocity. Thus, there are some vortices that are permanently pinned (at least over the simulated time). By contrast, for higher driving forces, whilst at any one time some vortices may be stationary, no vortices are permanently pinned. These data confirm earlier findings of Spencer and Jensen[11] employing a simpler model. For clarity, Fig. 3 does not distinguish between these two types of PF.

In the OPF regime, where the topological defect density, n_{d}, is lower than for the static system, we observe that the instantaneous velocity distribution shows no peak at zero

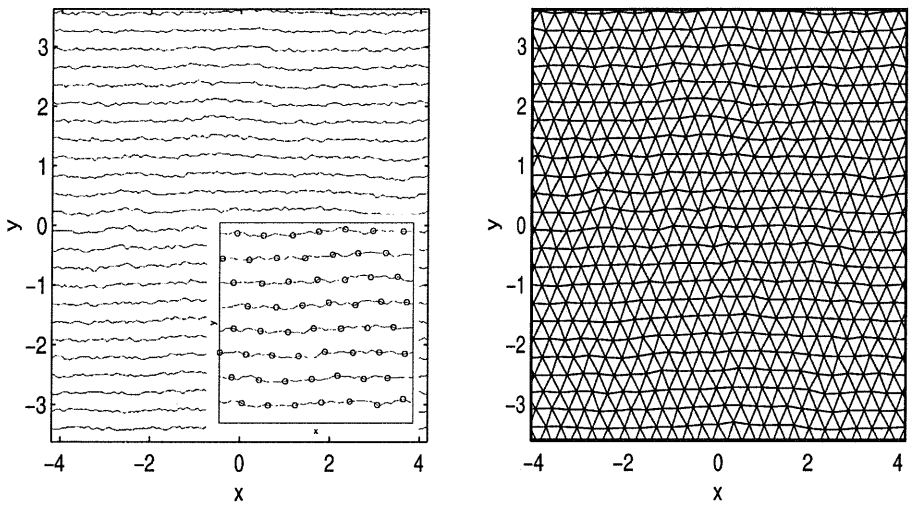

FIG. 5. The moving Bragg glass. Left: Histogram of vortex positions. The driving force is acting from left to right along the x direction, and vortices move in rough channels, like beads on a string. The inset shows a slightly enlarged version of the channels and positions of vortices for one time step are shown as circles. Right: Delaunay configuration of one snap shot of the same system. Although the channels in the left plot are rough, there are no topological defects in the moving Bragg glass.

velocity (i.e., all vortices are in motion), whereas this is not the case for both types of PF described in the last paragraph. Faleski, Marchetti, and Middleton[26] used the term crinkle flow to describe motion of vortices via correlated displacements of patches of vortices. Our observations of OPF suggest that the definition used here for OPF ($n_d < n_d^{\text{static}}$) is equivalent to the definition of crinkle flow introduced by Faleski, Marchetti, and Middleton[26] (absence of a peak at zero velocity in the instantaneous velocity distribution).

D. Decoupled channels

For sufficiently strong pinning and intermediate driving forces (Fig. 3) we find that vortices arrange in lines orientated along the direction of the driving force (Fig. 4). These lines move with different velocities in the direction of the driving force. This type of motion is described in detail in Sec. IV and is called decoupled channel motion.

E. Coherently moving structure

We observe two different kinds of coherently moving structures: (i) either a MBG (Ref. 14), which is free of topological defects (Fig. 5), or (ii) a hexagonal system similarly aligned with the direction of the driving force but with a few dislocations (Fig. 6). Both configurations move elastically, i.e., each vortex keeps its nearest neighbors for all times.

For strong pinning ($F_{\text{rms}}^{\text{vp}} \gtrsim 0.8 f_0$) and increasing driving force the transition from the decoupled channel regime to a coherently moving structure results in a MBG if the groups of coupled channels have the same vortex line density (see Sec. IV B). If the groups of coupled channels have different line densities then the dislocations between them are frozen into the coherently moving structure. For weak pinning ($F_{\text{rms}}^{\text{vp}} \lesssim 0.8 f_0$) the vortices do not move in decoupled channels for intermediate driving forces, and the system changes directly from OPF to a coherently moving structure. Again, elastically-moving systems with and without topological defects are observed. Our data from simulating current-voltage characteristics with increasing driving force suggest that the configuration at high driving forces is usually a hexagonal system aligned with the driving force with a few dislocations. However, a MBG configuration is occasionally observed.

The coherently moving structures we observe are always aligned with the direction of the driving force for pinning strengths $\gtrsim 0.8 f_0$. For smaller pinning strengths, configurations develop occasionally, which are not aligned with the driving force. It has been argued[16,18,27,28] that this alignment minimizes power dissipation, and our results are in agreement with other numerical investigations[9,10] in which the high-velocity configurations are generally aligned with the driving force.

For a MBG we find peaks at multiples of the washboard frequency $\omega_0 = 2\pi \langle v_{\text{cm}} \rangle / a_0$ in the Fourier spectrum of the center-of-mass velocity $v_{\text{cm}}(t)$ of the system, where $\langle\rangle$ denotes a time average and a_0 is the lattice constant of the vortex lattice. Whereas this temporal periodicity is not existent for the velocity of an individual vortex, we also find it in the energy of the system. Clear peaks in the Fourier spectrum can be observed up to frequencies of $\approx 100\omega_0$. For a single particle the washboard frequency is observable if it slides through a periodic potential. Here, we have a random poten-

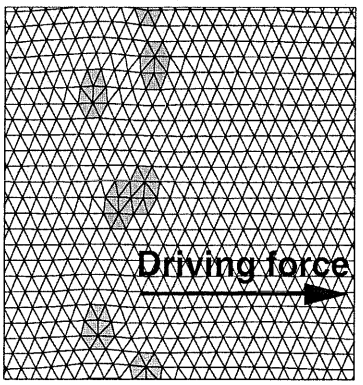

FIG. 6. A coherently moving structure with six dislocations (12 topological defects).

tial, but a periodic system. One thus finds the washboard frequency in observables that depend on all vortices, such as the center-of-mass velocity or the energy, but not for individual vortices. The washboard frequency has been found experimentally in ac (Refs. 29–31) and dc (Ref. 32) measurements, and numerically[12] in a similar regime.

In summary, we observe occasionally a MBG at high driving forces, but most of the final configurations are hexagonal systems aligned with the driving force with a few dislocations pairs. However, it could well be that finite temperatures or larger systems would favor the creation of a MBG at high driving forces: as yet, it is not clear what is the "dynamic ground state" of these systems. Our data cannot be used to decide whether a MBG exists in two dimensions or whether the MTG is the only stable phase,[16,18] since for a system of a given size if the velocity is sufficiently large then all channels couple and appear to be a MBG. Another open question is whether periodic boundary conditions can favor a reordering of a disordered vortex system.[33] The exploration of these questions is computationally expensive though new methods for evaluating interactions in the system may make this feasible.[19,34]

IV. DECOUPLED CHANNELS

This section describes a plastic mode of motion that, due to its quite different properties, is separated from the Sec. III C on turbulent plastic flow. As visible in the dynamic phase diagram in Fig. 3 the decoupled channels are only observed for sufficiently strong pinning.

Increasing the driving force (which acts in the x direction) from the turbulent plastic flow regime further, transforms the time-averaged velocity distribution from a broad peak as observed for turbulent plastic flow to several clearly distinct peaks as shown in Fig. 4(a). In Fig. 4(b) four different velocity levels are visible, each of these corresponding to one peak in the velocity histogram. Thus, vortices move in four groups of coupled channels and, within a group, all channels travel with a constant velocity in the direction of the driving force. Plot 4(c) shows the lattice structure of (b) in a two-dimensional projection. Vortices with more or less than six nearest neighbors are highlighted by a gray shade. We see that the groups of coupled channels are separated from each other by one 5-7 dislocation (a pair of vortices one having 5 and the other 7 nearest neighbors).

Plot 4(d) shows the initial (●) and final (×) positions of vortices in the frame of reference of one of the vortices in group C, and the initial and final positions are connected by a straight line, demonstrating that vortices never change the channels in which they move. This is a particularly interesting point since the moving glass theory[18] assumes that the topological defects (which are hard to treat analytically) between groups of coupled channel do not destroy transverse periodicity. Thus, the observation that these topological defects do not introduce chaotic motion of vortices and that the defects just decouple the different channels supports the theory of Giamarchi and Le Doussal.[18]

A series of runs shows that generally for larger driving forces the number of channels (and thus the size of each group) that are coupled and move with the same velocity increases, until the system shows elastic motion. For decreasing driving forces the number of coupled channels decreases until each group of coupled channels exists of only one or two channels. For even smaller driving force, the systems exhibit turbulent plastic flow.

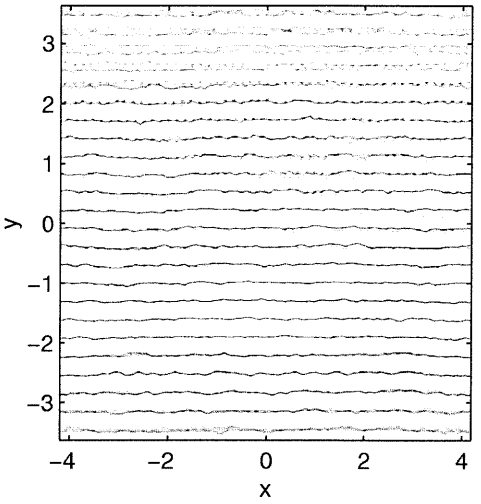

FIG. 7. This plot shows for the decoupled channel regime in which areas of the simulation vortices prefer to travel. On a 700×700 cell grid, a two-dimensional histogram of vortex positions has been created. The darker a cell, the more vortices have been counted within that cell over the duration of the simulation.

For the mixed regime shown in Fig. 3 we find that the mode of motion depends on the history of the system: Increasing the driving force for a system in the decoupled channel regime into the mixed regime results in motion in decoupled channels. On the other hand, reducing the driving force for a MBG into the mixed regime, yields elastic motion. For driving forces above the dotted line in Fig. 3 all systems show elastic motion and below the dash-dotted line all systems show smectic motion. The data suggest that both the MBG and the decoupled channels are metastable steady states that are separated by an energy barrier. In future we will explore whether finite temperatures are able to overcome this barrier.

Figure 7 shows an accumulation of vortex positions using a grid of 700×700 cells. It demonstrates that the channels in which vortices move are not strictly static but slightly broadened (see, for example, $y \approx 3$), although vortices never change channels. Further analysis in Sec. IV B shows that the 5-7 dislocations highlighted in Fig. 4(c) move with time in the x direction parallel to the driving force. Presumably this requires slight corrections of the static channels, which results in their blurred form visible in Fig. 7. This is supported by results given in Fig. 5 which show that for the MBG in the absence of dislocations the resulting channels are strictly static (and not blurred). This may indicate that the theoretical model[18] predicting strictly static channels for the MTG may be too simple.

Figure 8 shows the square modulus of the structure factor for two $\mathbf{k}$ vectors for the MTG. The large value of the (01) peak indicates the transverse order of the system. The small

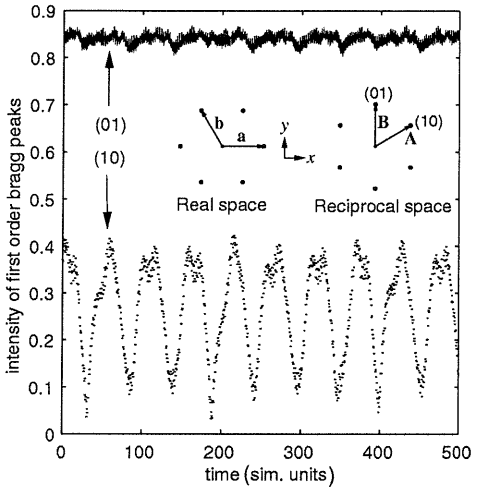

FIG. 8. Intensity of two Bragg peaks for the moving transverse glass shown in Fig. 4. The (01) peak is relative constant at a value of approximately 0.85 and it measures the order along the y direction. In contrast, the peak (10) measures also order along the x direction, and oscillates strongly. The variations are due to the different groups of coupled channels sliding past each other. The deviation of the (01) peak from 1.0 (as for a perfect lattice) is due to the roughness of the channels. The inset shows the lattice vectors used to label the peaks.

and oscillating (10) peak shows the strongly reduced order in the x direction. A time Fourier transform of the (10) signal reveals the frequencies with which the different groups overtake each other by one lattice spacing. This is exactly what is expected for a MTG in a finite system and is in agreement with the theoretical prediction[15–18] for the smectic regime that any peaks in the structure factor with a nonzero x-component should vanish in an infinitely large system.

The data shown are in agreement with the theoretically predicted moving smectic[15,16] that is also called MTG,[18] and decoupled channel regime.[17] A MTG has previously been identified by a numerical study of Olson, Reichhardt and Nori,[12] and the Delaunay triangulation of a snap shot of their system looks qualitatively like Fig. 4(c). Kolton, Domínguez and Grønbech-Jensen numerically found smectic states,[35] and earlier the numerical studies of Moon, Scalettar and T. Zimányi[9] on moving vortex systems suggested the possibility of phase slips of different channels. Further new results on the MTG are presented in the next two sections concerning the spatial distribution of vortex channel velocities depending on the pinning landscape (Sec. IV A), the mechanism of uncoupled channels sliding past each other (Sec. IV B), and the transverse depinning (Sec. IV C).

A. Dependence of the spatial velocity distribution on pinning landscape

We find a correlation between the particular pinning potential employed (representing details of the microstructure causing vortex pinning in the material) and the positions and velocities of the different groups of coupled channels. It should be noted that, although for the data shown in Fig. 4(b)

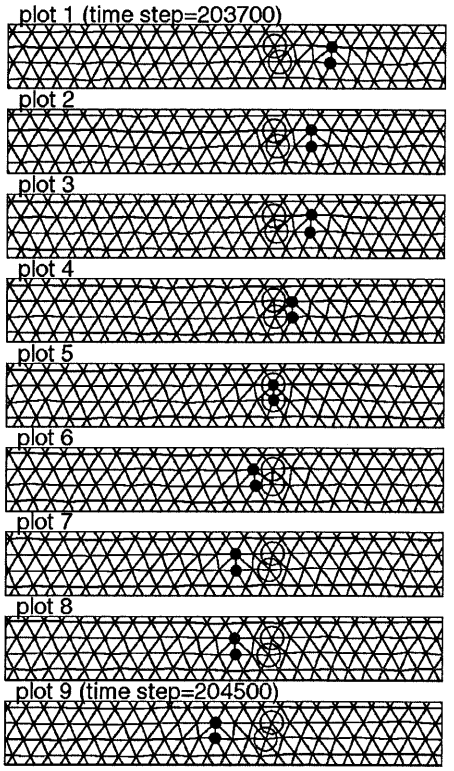

FIG. 9. Dislocation mediated phase slip in decoupled channel regime for different longitudinal vortex densities showing snap shots of 9 time steps. The open circles in each plot mark two fixed vortices, and the upper one defines the frame of reference. The Lorentz force acts from left to right. The upper two lines of vortices visible in each plot belong to group C in Fig. 4 and the lower to lines to group D. Thus, in the relative frame of reference, the lower two lines move to the left. The two black filled circles indicate topological defects in each snap-shot and represent a dislocation. These mediate the phase slip while moving to the left as can be seen by comparing the open circles in plots 1 and 9.

the vortices with the maximum velocity are located in the central region of the sample ($y \approx 0 \pm 1.5$), this is not an edge effect: for other samples the maximum is located at different y positions. Remarkably, in both the decoupled channel regime (Fig. 4) and the turbulent plastic flow regime (not shown here) the fastest flow is located in the same part of the simulated material.

It has been suggested[36] that the different velocities observed in the decoupled channel regime and shown in Fig. 4 may be related to the experimentally observed fingerprint effect.[4] In fact, it seems that for both the turbulent plastic flow and the decoupled channel regime the same areas of the pinning potential allow for better (or worse) pinning. This is not obvious since in the turbulent plastic flow regime vortices flow more or less individually along highly tortuous paths whereas in the decoupled channel regime they move in a much more correlated way.

B. Channel sliding mechanisms

Figure 4 shows that the number of vortices per line of vortices (the line density) differs from group to group by 1,

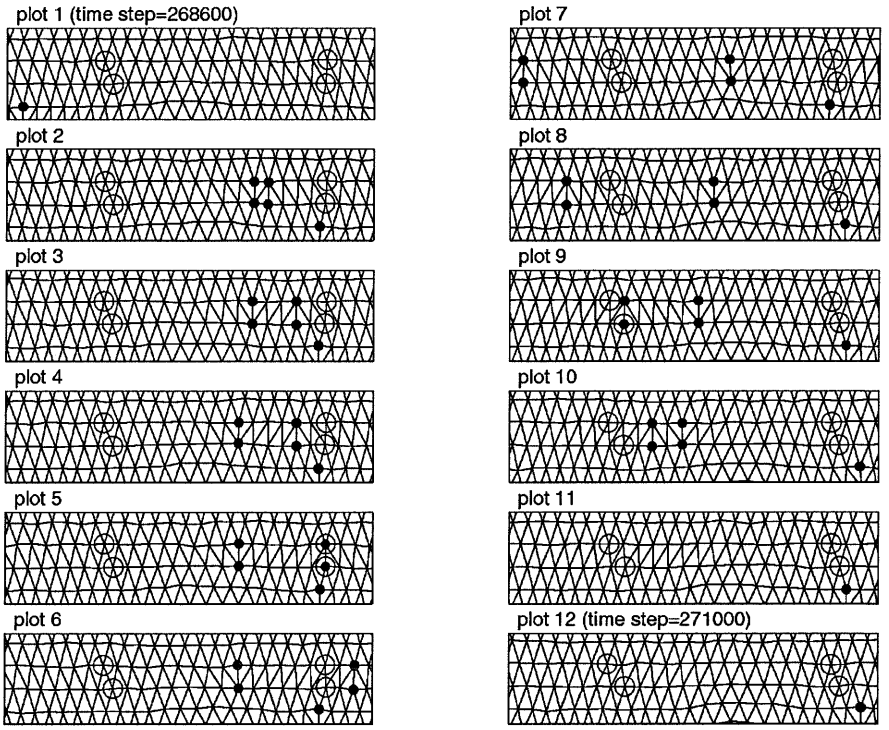

FIG. 10. Dislocation mediated phase slip in decoupled channel regime for equal longitudinal vortex densities. The open circles mark four fixed vortices and black filled circles show topological defects. Here, in the relative frame of reference, the lower two lines move to the right. The phase slip is realized by two dislocations consisting of a 5-7 and a 7-5-disclination pair (counting first the nearest neighbors for the upper disclination). These emerge from a pair-antipair creation process in plot 2. The 5-7-dislocation on the left moves to the left and the 7-5-dislocation to the right-hand side. In this process they allow the lower lines to pass a lattice spacing to the right. Between plots 6 and 7 the 7-5-dislocation leaves the simulation cell at the right-hand side and enters it again on the left-hand side. Finally, in plot 10, the two dislocations meet again and annihilate each other. The topological defect in the lowest row is not important here.

and exactly one dislocation between the groups is required to accommodate this difference [Fig. 4(c)]. In Fig. 9 a time series of Delaunay[24] triangulations of snap shots of a part of Fig. 4 is shown, demonstrating how a moving dislocation allows group C to move faster than group D.

Figure 10 shows this process for two neighboring channels having the same longitudinal vortex density. Again the phase slip is mediated by dislocations that travel along the channel. However, since initially there are no dislocations between the channels a dislocation pair is created. These dislocations travel away from each other, allowing the phase slip between the upper and lower two lines. When the dislocations meet again (due to periodic boundary conditions) they annihilate.

Only the two mechanisms shown in Figs. 9 and 10 have been observed. The situation with the same longitudinal vortex density has been observed less frequently that may indicate that this is energetically more expensive. However, in macroscopic systems the two mechanisms described are less distinguishable and may coexist: the local vortex line density differs around each of the dislocations in Fig. 10. Thus, the process shown in Fig. 9 may just be a more detailed study of the phase slipping process in Fig. 10 for each of the dislocations.

From a figure in the work of Olson, Reichhardt and Nori[12] we identify varying longitudinal vortex densities and Burgers vectors[37] parallel to the driving force, both in agreement with our results.

In conclusion, as far as we know, the detailed mechanism of decoupled channels moving past each other has been identified for the first time. The phase slip is mediated by disclination pairs which either exist between separate groups of coupled channels with locally different line densities of vortices, or the disclination pairs are created dynamically and in pairs when sufficient shear stress has built up. These results may help in finding a starting point for a theoretical description of the dynamics of dislocations, such as a Kosterlitz-Thouless[38] theory for nonequilibrium systems.

C. Transverse depinning

Following the theory of Giamarchi and Le Doussal,[14] at zero temperature, a nonanalytical response of the vortex system to a small transverse force is expected for the moving glass, i.e., for the MBG and the MTG. In agreement with our results in both the MBG and the MTG the existence of such transverse barriers have been observed in simulations.[9,10,39,40] The transverse depinning of the MBG has recently been described[39] and here we report on the transverse depinning of the MTG. We have found that the transverse depinning of a MTG may happen in two ways:

Mechanism A. At a certain strength of the transverse force (below the transverse depinning force), some vortices change the rows in which they have moved so far, such that after this first step the different groups of coupled channels *A*, *B*, *C*, and *D* (in Fig. 4) have the same number of vortices in each row. Then, all these rows move with the same velocity, i.e., the system has changed from a MTG to a MBG. This MBG does not (yet) move in the transverse direction. Only when the transverse driving force is increased even further, the system depins in the transverse direction, and moves elastically in the longitudinal and the transverse direction as described in Ref. 39.

Mechanism B. At the transverse depinning force the system rearranges plastically such that the rows of vortices (which are aligned with the x axis in Fig. 4) become orientated with an angle to the x axis after the change. The new direction of the rows is not the same as the direction of the total driving force (adding the small transverse force to the main driving force along the x axis).

We have found that the critical transverse force is higher for mechanism *A*. Our early investigations have shown that the transverse depinning of the MTG is an intricate matter and further studies are required to reveal under which circumstances mechanism *A* or *B* appears.

V. CONCLUSIONS

We have modeled the dynamics of vortices in two dimensions using overdamped Langevin dynamics with a logarithmic vortex-vortex interaction potential that includes a modified cutoff[19] to avoid introducing numerical artifacts into the simulation. We have computed a dynamic phase diagram as a function of pinning strength and driving force. We find pinned vortex systems, different kinds of turbulent plastic flow, and for large driving forces motion of vortices in rough channels along the direction of the driving force. Depending on pinning strength and driving force the motion in different channels can either be coupled or decoupled. These phases can be identified with the predicted MBG [Ref. 14] and the MTG [Ref. 15] as described in recent theoretical models.[14–18]

We have studied the MTG in detail and report on the dependence of the vortex channel velocities on the pinning landscape. We have identified how topological defects mediate the phase slip between channels moving with different velocities, and we have shown that vortices never change the channels in which they are moving, i.e., the dislocations in the system do not produce chaotic motion of vortices, thus preserving transverse periodicity. Together with the observed critical transverse force for the MTG and the MBG in these simulations, our findings strongly support the moving glass theory of Giamarchi and Le Doussal[18] that assumes that the dislocations in the MTG do not introduce additional effects that may destroy transverse periodicity (and thus the critical transverse force) in the MTG.

Our findings may also help in finding an extension to the Kosterlitz-Thouless[38] theory for nonequilibrium systems.

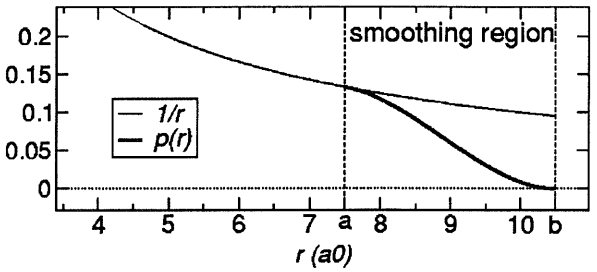

FIG. 11. Demonstrating the shape of the interpolating polynomial $p(r)$ (thick line) that smoothly reduces the vortex-vortex interaction force $f(r)$ to zero. For clarity we have chosen $f(r)=1/r$. The interpolation starts at the fading distance $a=7.5a_0$ and reduces the interaction force to zero at the cutoff distance $b=10.5a_0$, where a_0 is the average vortex lattice spacing. See text for details.

ACKNOWLEDGMENTS

We thank P. Le Doussal, A. R. Price, and S. Gordeev for helpful discussions. We acknowledge financial support from DAAD and EPSRC.

APPENDIX: SMOOTH CUTOFF

We employ a smooth cutoff for the vortex-vortex interaction following the ideas described in Ref. 19. Here we give details on the particular interpolating function we have chosen.

The vortex-vortex interaction has to be cutoff for distances greater than a cutoff distance b. Assume the interaction force is given by $f(r)$. For short-ranged interactions it is sufficient to use an interaction $\hat{f}(r)$ which is $f(r)$ for $r \leqslant b$ and zero otherwise:

$$\hat{f}(r)=\begin{cases} f(r), & r \leqslant b \\ 0, & r>b. \end{cases}$$

For long-ranged forces this approach results in artificial configurations.[19] However, those problems can be overcome by reducing $f(r)$ smoothly to zero near the cutoff distance b. One needs to introduce another distance a, and a polynomial $p(r)$, such that $a<b$ and that $p(r)$ interpolates between $f(a)$ at a and and zero at b:

$$\hat{f}(r)=\begin{cases} f(r), & r \leqslant a \\ p(r), & a<r \leqslant b \\ 0, & r>b. \end{cases}$$

It is required[19] that $\hat{f}(r)$ shows C^1 continuity at a and b, and its derivative at b to be zero:

$$f(a)=p(a), \tag{A1a}$$

$$p(b)=0, \tag{A1b}$$

$$\left.\frac{df}{dr}\right|_{r=a}=\left.\frac{dp}{dr}\right|_{r=a}, \tag{A1c}$$

$$\left.\frac{dp}{dr}\right|_{r=b}=0. \tag{A1d}$$

We have used a third-order polynomial

$$p(x)=\sum_{i=0}^{3} c_i x^i = c_3x^3+c_2x^2+c_1x+c_0$$

and the coefficients c_i are completely determined by Eqs. (A1a)–(A1d). Writing $f'(r)$ for $df/dr(r)$ one finds

$$\begin{pmatrix} c_3 \\ c_2 \\ c_1 \\ c_0 \end{pmatrix} = \frac{1}{(a-b)^3} \begin{pmatrix} f'(a)a-f'(a)b-2f(a) \\ -f'(a)a^2+3f(a)(a+b)-af'(a)b+2f'(a)b^2 \\ (2f'(a)a^2-af'(a)b-6f(a)a-f'(a)b^2)b \\ -f'(a)b^2a^2+3f(a)ab^2+f'(a)ab^3-b^3f(a) \end{pmatrix}.$$

The cutoff distance b is determined by geometrical constraints (see Sec. II A). We follow Ref. 19 and choose the distance $b-a$ over which the interaction is reduced to zero to be three lattice spacings, so that $a=b-3a_0$. In this work $f(r)\propto 1/r$. Figure 11 shows a schematic plot of the smooth cutoff and the interpolating polynomial.

To compute the potential energy of the system it is required to integrate $-p(x)$ to represent the smoothed interaction potential for $a<r<b$. The integration constant is determined by requiring continuity of the interaction potential at $r=a$.

[1] R. Thorel, J. Phys. (Paris) **34**, 447 (1973).
[2] S. Bhattacharya and M.J. Higgins, Phys. Rev. Lett. **70**, 2617 (1993).
[3] U. Yaron, P.L. Gammel, D.A. Huse, R.N. Kleiman, C.S. Oglesby, E. Bucher, B. Batlogg, D.J. Bishop, K. Mortensen, K. Clausen, C.A. Bolle, and F. De La Cruz, Phys. Rev. Lett. **73**, 2748 (1994).
[4] M.J. Higgins and S. Bhattacharya, Physica C **257**, 232 (1996).
[5] M.C. Hellerqvist, D. Ephorn, W.R. White, M.R. Beasley, and A. Kapitulnik, Phys. Rev. Lett. **76**, 4022 (1996).
[6] M. Marchevsky, J. Aarts, P.H. Kes, and M.V. Indenbom, Phys. Rev. Lett. **78**, 531 (1997).
[7] F. Pardo, F. de la Cruz, P.L. Gammel, E. Bucher, and D.J. Bishop, Nature (London) **396**, 348 (1998).
[8] A.-C. Shi and A.J. Berlinsky, Phys. Rev. Lett. **67**, 1926 (1991).
[9] K. Moon, R.T. Scalettar, and G.T. Zimányi, Phys. Rev. Lett. **77**, 2778 (1996).
[10] S. Ryu, M. Hellerqvist, S. Doniach, A. Kapitulnik, and D. Stroud, Phys. Rev. Lett. **77**, 5114 (1996).
[11] S. Spencer and H.J. Jensen, Phys. Rev. B **55**, 8473 (1997).
[12] C.J. Olson, C. Reichhardt, and F. Nori, Phys. Rev. Lett. **81**, 3757 (1998).
[13] A.E. Koshelev and V.M. Vinokur, Phys. Rev. Lett. **73**, 3580 (1994).
[14] T. Giamarchi and P. Le Doussal, Phys. Rev. Lett. **76**, 3408 (1996).
[15] L. Balents, M.C. Marchetti, and L. Radzihovsky, Phys. Rev. Lett. **78**, 751 (1997).
[16] L. Balents, M.C. Marchetti, and L. Radzihovsky, Phys. Rev. B **57**, 7705 (1998).
[17] S. Scheidl and V.M. Vinokur, Phys. Rev. E **57**, 2574 (1998).
[18] P. Le Doussal and T. Giamarchi, Phys. Rev. B **57**, 11 356 (1998).
[19] H. Fangohr, A. Price, S. Cox, P.A.J. de Groot, G.J. Daniell, and K.S. Thomas, J. Comput. Phys. **162**, 372 (2000).
[20] J.R. Clem, Phys. Rev. B **43**, 7837 (1991).
[21] J. Bardeen and M.J. Stephen, Phys. Rev. **140**, A1197 (1965).
[22] P.M. Chaikin and T.C. Lubensky, *Principles of Condensed Matter Physics* (Cambridge University Press, Cambridge, 1995).
[23] A. van Otterlo, R.T. Scalettar, and G.T. Zimanyi, Phys. Rev. Lett. **81**, 1497 (1998).
[24] M. de Berg, M. van Kreveld, M. Overmars, and O. Schwarzkopf, *Computational Geometry* (Springer Verlag, Berlin, 1997).
[25] T. Giamarchi and P. Le Doussal, Phys. Rev. Lett. **72**, 1530 (1994).
[26] M.C. Faleski, M.C. Marchetti, and A.A. Middleton, Phys. Rev. B **54**, 12 427 (1996).
[27] A. Schmid and W. Hauger, J. Low Temp. Phys. **11**, 667 (1973).
[28] J. Müllers and A. Schmid, Ann. Phys. (Leipzig) **4**, 757 (1995).
[29] S. Bhattacharya, J.P. Stokes, and M.J. Higgins, Phys. Rev. B **43**, 1835 (1991).
[30] J.M. Harris, N.P. Ong, R. Gagnon, and L. Taillefer, Phys. Rev. Lett. **74**, 3684 (1995).
[31] J.M. Harris, K. Krishana, N.P. Ong, R. Gagnon, and L. Taillefer, J. Low Temp. Phys. **105**, 877 (1996).
[32] Y. Togawa, R. Abiru, K. Iwaya, H. Kitano, and A. Maeda, cond-mat/0009476 (unpublished).
[33] V. Vinokur (private communication).
[34] S.J. Cox, G.J. Daniell, H. Fangohr, and A.M. Robinson (unpublished).
[35] A.B. Kolton, D. Domínguez, and N. Grønbech-Jensen, Phys. Rev. Lett. **83**, 3061 (1999); Phys. Rev. B **62**, R14657 (2000); Phys. Rev. Lett. **86**, 4112 (2001).
[36] S. Bhattacharya (private communication).
[37] N.W. Ashcroft and N.D. Mermin, *Solid State Physics* (Saunders College, Orlando, 1976).
[38] J.M. Kosterlitz and D.J. Thouless, J. Phys. C **6**, 1181 (1973).
[39] C.J. Olson and C. Reichhardt, Phys. Rev. B **61**, R3811 (2000).
[40] H. Fangohr, P.A.J. de Groot, and S.J. Cox, Phys. Rev. B **63**, 064501 (2001).